MOLECULAR AND CELLULAR BIOLOGY, Jan. 2005, p. 847–853 Vol. 25, No. 2
0270-7306/05/$08.00+0 doi:10.1128/MCB.25.2.847–853.2005

Deafness and Cochlear Fibrocyte Alterations in Mice Deficient for the Inner Ear Protein Otospiralin

Benjamin Delprat,* Jérôme Ruel, Matthieu J. Guitton, Ghyslaine Hamard,† Marc Lenoir, Rémy Pujol, Jean-Luc Puel, Philippe Brabet, and Christian P. Hamel*

INSERM, U.583, Physiopathologie et Thérapie des Déficits Sensoriels et Moteurs, Institut des Neurosciences de Montpellier, Hôpital Saint-Eloi, Montpellier, France

Received 26 June 2004/Returned for modification 16 September 2004/Accepted 10 October 2004

In the cochlea, the mammalian auditory organ, fibrocytes of the mesenchymal nonsensory regions play important roles in cochlear physiology, including the maintenance of ionic and hydric components in the endolymph. Occurrence of human deafness in fibrocyte alterations underlines their critical roles in auditory function. We recently described a novel gene, *Otos*, which encodes otospiralin, a small protein of unknown function that is produced by the fibrocytes of the cochlea and vestibule. We now have generated mice with deletion of *Otos* and found that they show moderate deafness, with no frequency predominance. Histopathology revealed a degeneration of type II and IV fibrocytes, while hair cells and stria vascularis appeared normal. Together, these findings suggest that impairment of fibrocytes caused by the loss in otospiralin leads to abnormal cochlear physiology and auditory function. This moderate dysfunction may predispose to age-related hearing loss.

Within the cochlea, the mammalian auditory organ, mesenchymal nonsensory regions (i.e., the spiral limbus proximal to the cochlear axis and the spiral ligament forming the lateral wall of the cochlea) contain fibrocytes that play important roles in cochlear physiology. In the spiral ligament, these fibrocytes form distinct groups according to their location, morphological appearance, and marker expression, which suggest their functional specialization (26). Thus, the circumferentially oriented type III fibrocytes lining the otic capsule and the spindle-shaped type IV fibrocytes lateral to the basilar membrane package the cochlear content and buffer mechanical constraints generated by sound vibrations (8). The type I fibrocytes (behind the stria vascularis), tightly packed with collagen bundles, shape the curvature of the lateral wall. Type II fibrocytes (below the stria vascularis) and type V fibrocytes (above the stria vascularis) are rich in mitochondria and form many interdigitating processes, indicating high metabolic and exchange activities. Type I, II, and V fibrocytes and basal and intermediate cells of the stria vascularis are all interconnected with gap junctions (10). This gap-junctioned network is postulated to be involved in ion and water circulation, including potassium recycling (34). Potassium is indeed central to the cochlear physiology, since it is the charge-carrying ion for the sensory transduction. It is secreted by the marginal cells of the stria vascularis to maintain a very high concentration (150 mM) in the endolymph, the extracellular fluid bathing hair cell stereocilia. Recycling of potassium though the fibrocyte network is one of several processes that provide potassium to intermediate cells of the stria vascularis (28, 34). This permanent flux of potassium cycling in the cochlea generates the so-called "endocochlear potential " (+85 mV), which gives the main driving force for potassium entry into the sensory hair cell.

Progress in the functional characterization of the cochlear fibrocytes has been made with the discovery of proteins expressed in the nonsensory regions. In accordance with their role in ionic and water transport, fibrocytes express various combinations of ion and water channels, carbonic anhydrases II and III (3, 21, 25, 27, 30), as well as gap junction connexins 26, 30, and 31 (7, 12, 37). The findings that fibrocytes also express extracellular matrix proteins (15, 33, 35) and proteins involved in cell-cell signaling, such as bone and cartilage morphogens (2, 18, 20, 31) and the inner ear-specific cochlin, whose function is unknown (19), indicate a broader role and probably a diversity of specific functions that remain to be elucidated. The fact that the alteration of the fibrocyte integrity leads to pathology is an indication of their importance in inner ear physiology. Thus, mutations in some fibrocyte-expressed genes, such as those coding for the chloride-iodide transporter pendrin (6, 23) and cochlin, are responsible for the Pendred syndrome (5) and DFNA9 (19), respectively, and alteration of fibrocytes is observed in first steps of some age-related hearing loss models (9, 36).

We previously showed that, in rats, cochlear fibrocytes express a novel, 6.4-kDa protein that we called otospiralin because of its expression in spiral structures of the cochlea, i.e., the spiral ligament and spiral limbus (4). Otospiralin expression is largely restricted to the inner ear, with only trace amounts of mRNA detected by reverse transcription-PCR (RT-PCR) in brain (24) and the presence of the protein in the inner ear detected only by Western blotting (4). Today, the function of otospiralin remains elusive, although its conser-

* Corresponding author. Mailing address for Christian P. Hamel: INSERM U.583, Physiopathologie et Thérapie des Déficits Sensoriels et Moteurs, Institut des Neurosciences de Montpellier, Hôpital Saint-Eloi, BP 74103, 80, rue Augustin Fliche, 34295 Montpellier cedex 05, France. Phone: 33 499 636 010. Fax: 33 499 636 020. E-mail: hamel@montp.inserm.fr. Mailing address for Benjamin Delprat: INSERM U. 587, Génétique des Déficits Sensoriels, 25 rue du Dr Roux, 75724 Paris cedex 15, France. E-mail: delprat@pasteur.fr.

† Present address: INSERM U.567, Institut Cochin, 75014 Paris, France.

vancy from fish to mammals (13) is in accordance with the presence of hair cell organs (i.e., lateral line and cochlea) and thus with vibration detection. Antisense experiments with guinea pigs showed alteration of the cochlear fibrocytes and degeneration of the hair cells, demonstrating the involvement of otospiralin in auditory function (4). These results, along with the lack of known sequence homology, suggested an important and novel role for otospiralin in inner ear biology. We now report that *Otos*-invalidated mice show hearing impairment. Although the organ of Corti was ultrastructurally normal, some fibrocytes of the spiral ligament and spiral limbus were damaged, suggesting that otospiralin is important for the integrity of the cochlear fibrocytes and for normal performance of the cochlea.

MATERIALS AND METHODS

Targeting construction and generation of *Otos*$^{-/-}$ mice. An 8-kb HindIII 129/X1SvJ genomic fragment containing the entire *Otos* gene was isolated and subcloned into pBluescript SK (Stratagene). Subsequently, 1.5-kb EcoRI-StuI and 5.2-kb SphI-XhoI fragments flanking the 5′ and 3′ regions of *Otos*, respectively, were subcloned into pBluescript cut with XbaI and XhoI and modified by the introduction of an EcoRI-StuI-SalI-KpnI-BclI-SphI polylinker. The *LacZneo* cassette, containing a nuclear localization signal and neomycin under the control of the thymidine kinase (*tk*) promoter, was fused in frame after nucleotide 10 of the ATG of *Otos* (exon 2). The polyadenylation sequence from the pPolIIIlongneobpA plasmid was added to stabilize the mRNA. Finally, the herpes simplex virus *tk* gene (HSV-*tk*) was inserted downstream of the 5.2-kb SphI-XhoI fragment of the mouse DNA.

Embryonic development day 14.1 embryonic stem (ES) cells were transfected with the NotI-linearized plasmid DNA (25 μg) with a Bio-Rad Genepulser (230 V, 500 μF) and were subjected to Geneticin (150 mg/ml active; Life Technologies) and ganciclovir (2 μM; Roche) treatments. Homologous recombination events were identified by PCR using primers specific to the 5′ mouse genomic sequence, outside the region used in the targeting vector (5′-AGCCAGGGTA AGTAACAGAGAGTTGCTG-3′), and to the *LacZ* sequence (5′-GGTACGG GGTCTTCTACCTTTCTCTTCT-3′). Two properly targeted ES clones out of 624 were recovered. The homologous recombination event was confirmed by direct sequencing of the fragment with internal primers. The integrity of the 3′ genomic edge was checked with a 1.9-kb HindIII-SphI fragment as a probe, and that of the 5′ edge was checked with a 1.3-kb NcoI-DraIII fragment of the LacZ sequence as a probe. Two clones were injected into C57BL/6N blastocysts. Chimeras were mated to C57BL/6N strain for germ line transmission, which was confirmed by PCR using LacZ (5′-GGTACGGGGTCTTCTACCTTTCTCTTC T-3′) and mSG6ko5′S2 (5′-CAGAAACAGAAGCACTTATGAA-3′) primers.

To assess otospiralin mRNA expression in mice, RT-PCR was performed on cochlear RNA (Rneasy kit; QIAGEN) from 5-day-old animals with exon 2 forward (5′-ATGCAGCCCTGTCTGCTGTGGTGG-3′) and exon 4 reverse (5′-GTCCTCCTGGTAGGGAACATGGAA-3′) primers (270-bp amplicon). The inner ear-specific otoconin-95 (*Ocn-95*) transcript was amplified with 5′-GTGT GACAAGGCTGCTGTGGAGTGC-3′ and 5′-CTCCGTCTGGTGACTTGAG GCTTTG-3′ primers as a positive control (788-bp amplicon). The absence of the protein was tested by Western blotting using the polyclonal antibody SE3950.

X-Gal staining and histological analysis. Dissected inner ears were fixed for 40 min in 4% paraformaldehyde (PFA), stained with X-Gal buffer (0.4-mg/ml 5-bromo-4-chloro-3-indolyl-D-galactoside, 2 mM potassium ferricyanide, 2 mM potassium ferrocyanide, 4 mM $MgCl_2$ in phosphate-buffered saline [PBS]) overnight at 37°C. They were decalcified for 3 days in a 16.8% EDTA solution after the staining step. The stained inner ears were embedded in paraffin as described previously (4), sectioned (14 μm), and counterstained with eosin for histological analysis.

Immunohistological analysis. For cochleas, 21-day-old mice were decapitated under deep anesthesia (pentobarbital [Nembutal], 50 mg/kg), their cochleas were quickly removed, and they were pierced at their apex and fixed overnight in 4% PFA. They were then decalcified 4 days in 10% EDTA, dehydrated in ethanol, cleared, and embedded in paraffin. Sections (7 μm) were deparaffinized, blocked in 30% goat serum, and incubated with SE3950 antiotospiralin antiserum diluted at 1/400. Bound primary antibodies were revealed by fluorescence using fluorescein isothiocyanate-conjugated secondary antibody (1/100).

Functional assessment: surgical procedure. *Otos*$^{+/+}$ (n = 10) and *Otos*$^{-/-}$ (n = 10) mice were anesthetized with an intraperitoneal injection of a 6% sodium pentobarbital solution (Sanofi, Montpellier, France) at 0.3 ml/kg of body weight and artificially breathed with a respirator (NBS NarcoBio-Systems). Rectal temperature was measured with a thermistor probe to control and maintain the body temperature at 38.5 ± 1°C, using a heated underblanket. Heart rate (normal range 260 to 330 per min) was monitored with an oscilloscope via electrocardiogram electrodes.

The pinna and the external meatus were resected bilaterally to the level of the tympanic annulus, and the animal was mounted in the head-holder of a stereotaxic apparatus to expose the bulla. A ventral approach was used to visualize the cochlea. Then a silver recording electrode was placed on the round window membrane of the cochlea. A reference electrode was inserted into the neck musculature.

Electrophysiology: gross cochlear and auditory nerve potentials. Cochlear potentials were elicited with tone bursts of a 1-ms rise/fall time and a 9-ms total duration generated by an arbitrary function generator (type 9100R; LeCroy Corporation, Chestnut Ridge, N.Y.). The signals were passed through a programmable attenuator and presented to the ear in a free field via a JBL 075 earphone (JBL, Northridge, Calif.). Ten frequencies were tested (2, 4, 6, 8, 10, 12, 16, 20, 26, and 32 kHz), with increasing levels of 5 dB from a 0- to 100-dB sound pressure level (SPL). The rate of presentation was 10 bursts per s. Cochlear responses were amplified (gain, 2,000) by a differential amplifier (Grass P511K), averaged (256 samples), and saved on a Pentium PC computer (100 Mhz; Dell Dimension). The stored potentials could then be digitally filtered with a low-pass setting at 2.5 kHz to measure the compound action potential (CAP) of the auditory nerve, and the summating potential (SP) reflecting the summed intracellular *dc* receptor potential, mainly generated by the inner hair cells (IHCs) (1). Filtering cochlear potentials with a band-pass filter centered on the frequency of tone burst stimulation allows extraction of the cochlear microphonic (CM) reflecting the summed intracellular *ac* receptor potential mainly generated by outer hair cells (OHCs) (17).

Statistical analysis of the data. To evaluate the significance of the functional difference between *Otos*$^{+/+}$ and *Otos*$^{-/-}$ mice, statistical tests were performed on Sigmaplot 2000 for Windows (version 6.1). All comparisons between means were performed with Student's paired two-tail t tests. The data values are expressed as means ± standard error.

TEM. For transmission electron microscopy (TEM), following the last electrophysiological test, animals were heavily anesthetized and the cochleas were quickly removed and perfused with a freshly prepared fixative containing 3.5% glutaraldehyde in sodium cacodylate buffer (0.1 M, pH 7.2). They were rinsed in cacodylate buffer, postfixed in 2% osmic acid for 2 h, rinsed twice again before dehydration, and embedded in Spurr resin at 70°C. Blocks were trimmed to separate the different cochlear coils and remounted for transverse sections. Semithin sections were examined in Nomarski optics before cutting of thin sections (80 to 100 nm) with a Leica-Reichert ultra-microtome. Grids, counterstained with uranyl acetate and lead citrate, were observed with a transmission electron microscope (Hitachi 7100). Three series of sections were taken from each block (two blocks per coil) so as to thoroughly examine at least six different levels of the organ of Corti per cochlea.

SEM. For scanning electron microscopy (SEM), after decapitation of the animal under deep anesthesia (pentobarbital, 50 mg/kg), cochleas were removed from the temporal bone and perfused with a fixative solution of 2.5% glutaraldehyde in 0.1 M pH 7.3 phosphate buffer and then immersed in the same fixative solution for 2 h. Then, the otic capsule was dissected out. The stria vascularis and the tectorial and Reissner membranes were removed. After being rinsed in the phosphate buffer, the samples were dehydrated in a graded series of ethanol (30 to 100%), critical point dried in CO_2, coated with gold palladium, and observed with a Hitachi S4000 microscope.

Antibody production. The peptide corresponding to amino acids 22 to 33 at the N terminus of the peptide signal-cleaved mouse otospiralin (NH_2-KPMPEE ADPHTQC-COOH) was coupled to keyhole limpet hemocyanin and injected into rabbits for antiserum production (Eurogentec, Seraing, Belgium). Antiserum SE3950 was obtained, and its specificity was checked by immunoblot analysis using the preimmune serum as a negative control.

Western blotting. Tissues were harvested in cold PBS and homogenized in sample buffer (11), and the lysate was centrifuged to remove detergent-insoluble material and separated by 16.5% polyacrylamide sodium dodecyl sulfate-polyacrylamide gel electrophoresis in Tris-Tricine (22). After gel electrophoresis, proteins were transferred electrophoretically to nitrocellulose membranes. Blots were incubated with SE3950 antiotospiralin antibody diluted at 1/1,000 according to Towbin et al. (32) and revealed by chemiluminescence using a peroxidase-conjugated secondary antibody (Boehringer Mannheim, Mannheim, Germany).

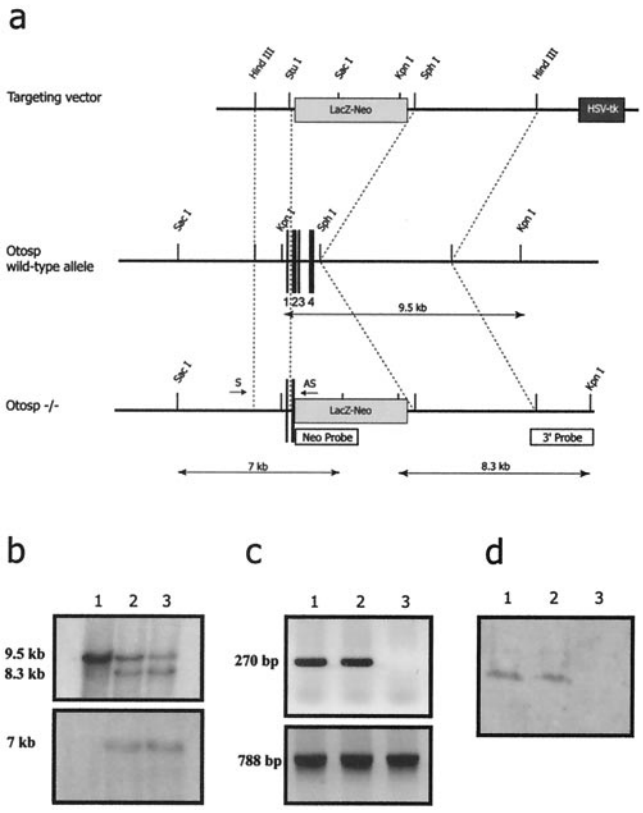

FIG. 1. Targeted deletion of the mouse *Otos* gene. (a) Construction of the deleted allele for the mouse *Otos* gene. (Top) Targeting vector containing the *LacZneo* and HSV-tk cassette. (Middle) Restriction map of the *Otos* locus. The four exons of *Otos* are numbered. (Bottom) Restriction map of the *Otos* locus after homologous recombination. (b) Southern blot analysis of ES cell genomic DNA digested with KpnI (top) or SacI (bottom). For KpnI digestion, the 9.5-kb fragment corresponds to the wild-type allele and the 8.3-kb fragment corresponds to the targeted allele. For SacI digestion, the 7-kb fragment corresponds to the targeted allele. (c) RT-PCR analysis of the inner ear showing the presence of the *Otos* transcript (top) in the $Otos^{+/+}$ (lane 1) and $Otos^{+/-}$ (lane 2) mice but not in $Otos^{-/-}$ mice (lane 3). Amplification of the otoconin-95 transcript was observed in the three genotypes (bottom). (d) Western blot analysis of the inner ear showing the presence of otospiralin in the $Otos^{+/+}$ (lane 1) and $Otos^{+/-}$ (lane 2) mice but not in $Otos^{-/-}$ mice (lane 3).

A polypeptide range marker was used for calibration (Bio-Rad, Richmond, Calif.).

Animal handling. The care and use of animals followed the animal welfare guidelines of the Institut National de la Santé et de la Recherche Medicale, under the approval of the French Ministère de l'Agriculture et de la Forêt. All efforts were made to minimize the number of animals used and their suffering.

RESULTS

Targeted disruption of the *Otos* gene. A λ phage containing the entire mouse *Otos* gene was isolated by screening a λ FIX II genomic DNA library derived from a 129/X1SvJ mouse strain. The restriction enzyme map was established (Fig. 1a). We constructed a vector by replacing most of the *Otos* coding sequence, including part of exon 2 and exons 3 and 4, with a neomycin–β-galactosidase (β-Gal) cassette. After electroporation into ES cells, two homologous recombinants were identified by PCR and confirmed by Southern hybridization using two probes, including one outside the vector (Fig. 1b). Both ES clones were used to generate chimeric mice by injection into mouse blastocysts. The chimeras were mated to C57BL/6N mice, and germ line transmission was confirmed by PCR analysis of tail DNA from F_1 progeny. Mating of heterozygous male and female mice generated F_2 progeny with the three genotypes in normal proportions (23% homozygous mutant, 51% heterozygous, and 26% wild-type mice) indicating that the absence of otospiralin is not embryonic lethal. The absence of otospiralin expression in the F_2 homozygous mutant mice was confirmed by RT-PCR (Fig. 1c) and Western blotting (Fig. 1d). $Otos^{-/-}$ mice exhibited neither growth development nor gross anatomy differences compared with their $Otos^{+/+}$ and $Otos^{+/-}$ counterparts.

Otospiralin is expressed in fibrocytes of the inner ear. To assess otospiralin expression in the inner ear in mice, we processed whole-mount $Otos^{+/-}$ cochleas for β-galactosidase activity. β-Gal staining was confined to fibrocytes of the spiral prominence in the spiral ligament and to those of the apical and basal borders in the limbus (Fig. 2a). Consistent with this staining, the immunofluorescence signal was detected in the fibrocytes of the spiral limbus and spiral ligament, although to a larger extent (Fig. 2b), suggesting that either the immunofluorescence test was more sensitive than the β-Gal staining or a certain amount of the protein is transported at distance from its synthesis site. Overall, these results indicated that activation of the otospiralin promoter and production of the protein itself did occur in fibrocytes of the inner ear. By Western blotting, the protein was found only in the cochlea and not in other tissues, including brain, cerebellum, spinal cord, eye, muscle, heart, liver, kidney, spleen, testis, lung, and thyroid (not shown), suggesting that otospiralin could exert a specific function in the inner ear.

***$Otos^{-/-}$* mice display hearing impairment.** To evaluate whether otospiralin is required for hearing, we performed a CAP audiogram of F_2 and F_3 $Otos^{-/-}$ mice on a mixed (50:50) 129 Olahsd:C57BL/6N genetic background. All mice were less than 3 months old to avoid the age-related hearing loss that occurs in C57BL/6N and 129 Olahsd-related strains (39). $Otos^{-/-}$ mice had a normal Preyer reflex and no sign of vestibular dysfunction (nystagmus or dizziness). However, comparison with wild-type mice revealed that CAP thresholds in $Otos^{-/-}$ mice were significantly ($P < 0.001$) increased over the entire frequency range (2 to 32 kHz). The mean ± standard error averages of CAP thresholds across frequency were 28.13 ± 3.97 dB ($n = 10$) in wild-type $Otos^{+/+}$ mice versus 47.04 ± 4.65 dB ($n = 10$) in $Otos^{-/-}$ mice. We further analyzed the CAP and CM amplitude and N1 latency at 10 kHz. A clear reduction of CAP and CM amplitude (Fig. 3b and d; $n = 10$) and a slight increase of N1 latency (Fig. 3c; $n = 10$) were observed at all intensities of tone-burst stimulation. To facilitate comparison between wild-type and $Otos^{-/-}$ mice, the CAP and CM amplitudes were combined across intensities (100 to 40 dB) to provide an overall mean for each group of mice expressed as the percentage of the wild-type mean value. Based on this calculation, $Otos^{-/-}$ mice showed reductions of 59.5 and 78.5% for CAP and CM amplitude, respectively. Altogether, these results show a global alteration in signal transmission in $Otos^{-/-}$ mice.

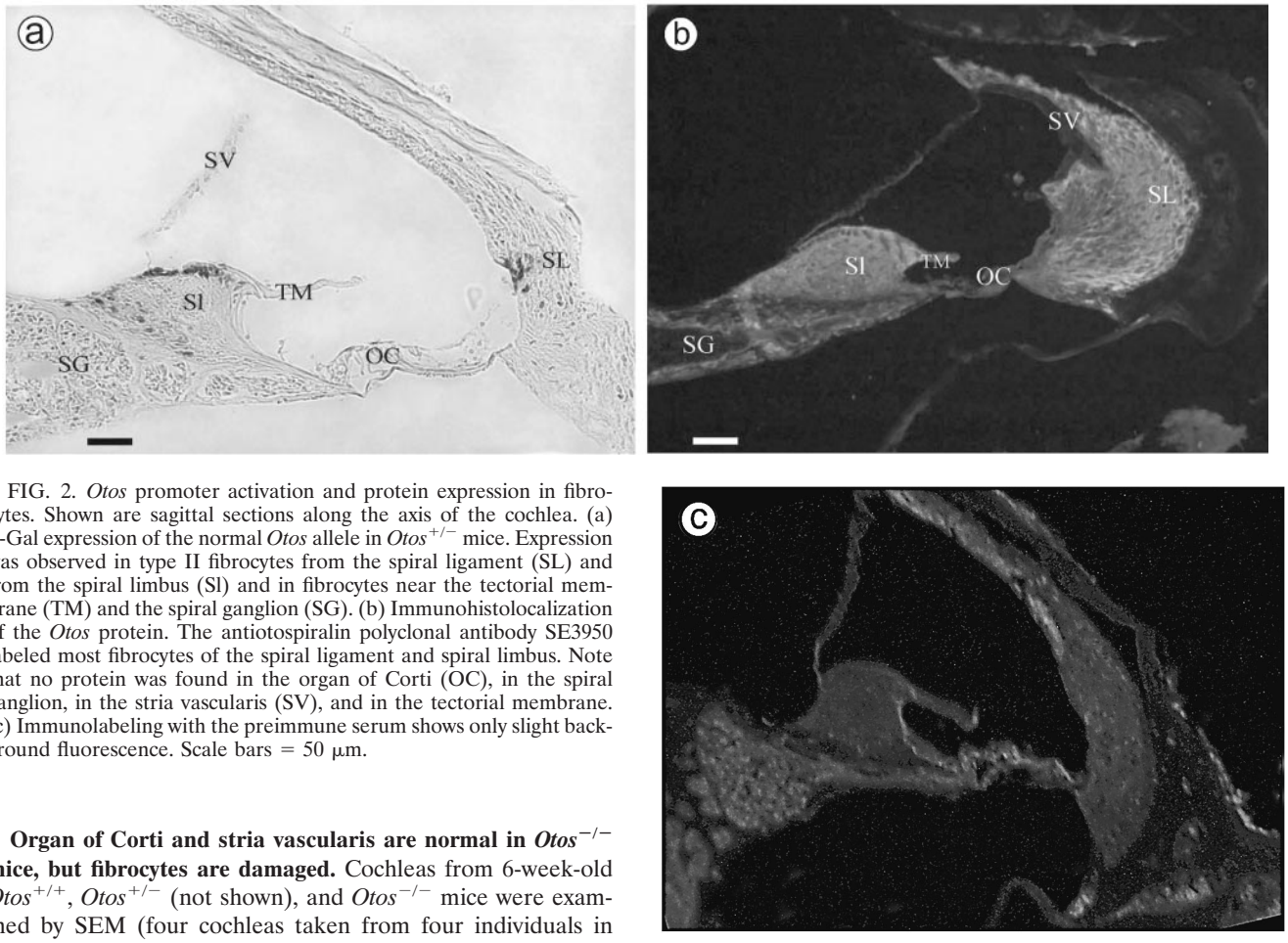

FIG. 2. *Otos* promoter activation and protein expression in fibrocytes. Shown are sagittal sections along the axis of the cochlea. (a) β-Gal expression of the normal *Otos* allele in $Otos^{+/-}$ mice. Expression was observed in type II fibrocytes from the spiral ligament (SL) and from the spiral limbus (Sl) and in fibrocytes near the tectorial membrane (TM) and the spiral ganglion (SG). (b) Immunohistolocalization of the *Otos* protein. The antiotospiralin polyclonal antibody SE3950 labeled most fibrocytes of the spiral ligament and spiral limbus. Note that no protein was found in the organ of Corti (OC), in the spiral ganglion, in the stria vascularis (SV), and in the tectorial membrane. (c) Immunolabeling with the preimmune serum shows only slight background fluorescence. Scale bars = 50 μm.

Organ of Corti and stria vascularis are normal in $Otos^{-/-}$ mice, but fibrocytes are damaged. Cochleas from 6-week-old $Otos^{+/+}$, $Otos^{+/-}$ (not shown), and $Otos^{-/-}$ mice were examined by SEM (four cochleas taken from four individuals in each group) and TEM (three cochleas taken from three individuals in each group). The cellular architecture of the organ of Corti in $Otos^{+/+}$ and $Otos^{-/-}$ mice was normal (Fig. 4a and c), with a single row of IHCs and three rows of OHCs separated by the pillar cells. We observed in both groups a few missing hair cells scattered throughout the cochlear spiral, which had no pathological significance. On both types of hair cells, the structure and orientation of the hair bundles were unaffected by the absence of *Otos*. Similarly, the stria vascularis was morphologically normal in $Otos^{-/-}$ mice, with deep infoldings of the basal plasma membrane, numerous mitochondria in the marginal cells, and normal-looking intermediate and basal cells (Fig. 4b and d).

However, some fibrocytes of the spiral limbus and spiral ligament were damaged (Fig. 5). While $Otos^{-/-}$ type II fibrocytes (within and nearby the spiral prominence) had, like their wild-type counterparts, numerous infoldings of the cell membrane, they showed shrinkage of their cytoplasm with concomitant larger extracellular spaces around them than those of wild-type animals (Fig. 6a and b). In addition, their cytoplasm exhibited vacuoles that looked empty to the electron rays. Type IV fibrocytes (in the triangular space inferior to the basilar crest) also had larger extracellular spaces but did not show large vacuoles. These extended extracellular spaces were also observed in some fibrocytes of the spiral limbus (Fig. 6c and d). In contrast, type I and III fibrocytes were present and exhibited normal structure (not shown).

DISCUSSION

To get insight into the role of otospiralin in the inner ear, we have generated a mouse model in which most of the coding sequence was deleted. $Otos^{-/-}$ mice develop normally and do not exhibit severe hearing loss or vestibular syndrome. Nevertheless, functional investigations revealed that there is an auditory defect with no frequency predominance. This defect is not linked to ultrastructural damage of hair cells or stria vascularis but to the alteration of the fibrocytes in the mesenchymal parts of the cochlea.

The auditory impairment observed in the $Otos^{-/-}$ mice is clearly different from the severe deafness seen in the guinea pig cochleas treated with otospiralin antisense oligonucleotides (4). In the latter experiment, hair cells were lost while they remained intact in the $Otos^{-/-}$ mice. Such a difference may rely upon long-term adaptation of the cochlea to the congenital absence of otospiralin in the $Otos^{-/-}$ mice or, alternatively, be linked to the fact that oligonucleotides in antisense experiments may have targeted, in addition to otospiralin, another factor important for hair cell survival. Nonetheless, damage to the mesenchymal fibrocytes of the spiral ligament and spiral limbus, which was the only histological abnormality observed in the $Otos^{-/-}$ mice, was strictly identical to that observed in guinea pig cochleas treated with otospiralin antisense oligonu-

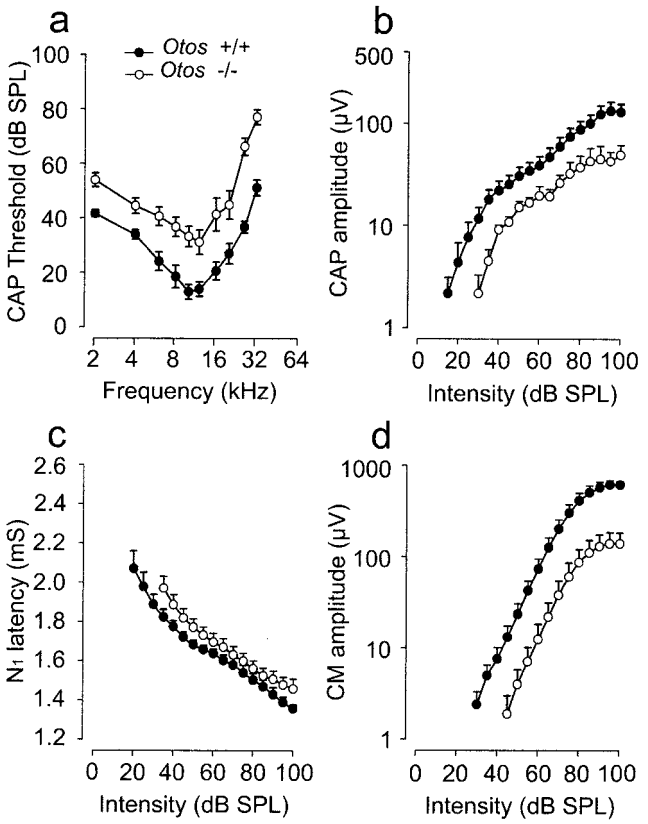

FIG. 3. *Otos*$^{-/-}$ mice show moderate deafness. Shown are the results of functional investigations of <3-month-old F_2 and F_3 *Otos*$^{-/-}$ mice compared with *Otos*$^{+/+}$ wild-type mice at the same age. Sound stimulation generates a CAP. (a) CAP threshold plotted as a function of the sound frequency showing that *Otos*$^{-/-}$ mice have an increase in the CAP threshold over the whole frequency range, indicating a loss in sound sensitivity. (b) CAP amplitude plotted as a function of sound intensity showing that *Otos*$^{-/-}$ mice have a decrease in the CAP amplitude for all intensities. (c) CAP N1 latency plotted as a function of sound intensity showing that *Otos*$^{-/-}$ mice have an increase in the CAP latency for all intensities. (d) CM amplitude measured from the round window and plotted as a function of sound intensity showing that *Otos*$^{-/-}$ mice have an important reduction in the amplitude compared to *Otos*$^{+/+}$ mice.

cleotides (4), indicating that this is a characteristic feature of the lack of otospiralin.

The fact that cytoplasmic alterations predominate in those fibrocytes which produce otospiralin (i.e., type II in spiral ligament and some fibrocytes of spiral limbus, as seen from the otospiralin promoter activity) suggests that the lack of otospiralin exerts a direct effect on fibrocytes themselves. There are examples of animal models in which fibrocyte degeneration is due to a molecular defect involving primarily fibrocytes with relatively few structural alterations in the neurosensory epithelium (14, 16, 38). These fibrocyte alterations may lead to severe auditory impairment, which has been attributed to important modifications of the production and composition of the endolymph. In the *Slc12a2*$^{-/-}$ mice (14), which are deficient for the Na^+-K^+-$2Cl^-$ cotransporter that is normally expressed in type II and IV fibrocytes and stria vascularis, there is a collapse of the Reissner membrane, indicating that the volume of the endolymph is considerably decreased, presumably because of

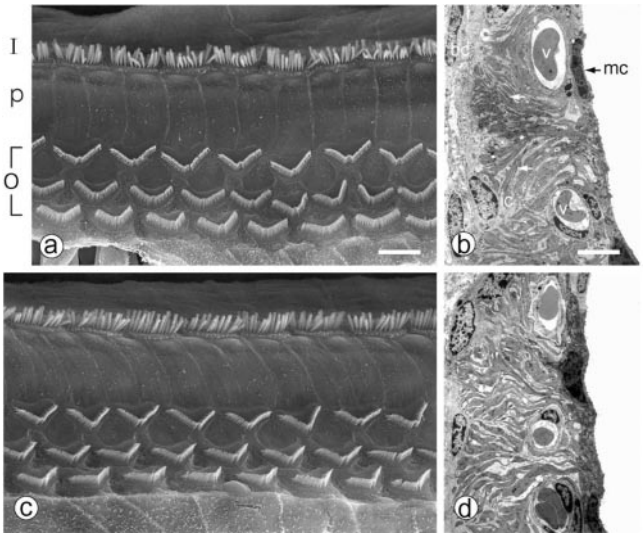

FIG. 4. *Otos*$^{-/-}$ mice have a normal organ of Corti and stria vascularis. (a and c) Scanning electron micrographs illustrating the structure of the organ of Corti in wild-type (a) and *Otos*-deficient (c) 6-week-old mice. The organization of the IHC (I) and OHC (O) hair bundles and pillar cells (p) is normal in both specimens, with one row of hair bundles for the IHCs and three rows for the OHCs. (b and d) Transmission electron micrographs of wild-type (b) and *Otos*-deficient (d) mice. In both cases, the stria vascularis shows a typical appearance with numerous blood vessels (v) and prominent basolateral infoldings of the marginal cells (mc) interlacing with intermediate cell (ic) digitations (arrows) and normal basal cells (bc). Scale bars = 10 μm.

insufficient K^+ secretion. In mice deficient for the Pou transcription factor Pou3f4, which in wild-type animals is only expressed in fibrocytes of the spiral ligament and spiral limbus (16, 38), there is remarkable damage to type II and IV fibrocytes, while the organ of Corti remains normal. As in *Otos*$^{-/-}$ mice, fibrocytes show larger extracellular spaces. In addition, in the *Pou3f4*$^{-/-}$ model, scarcity of mitochondria and of mem-

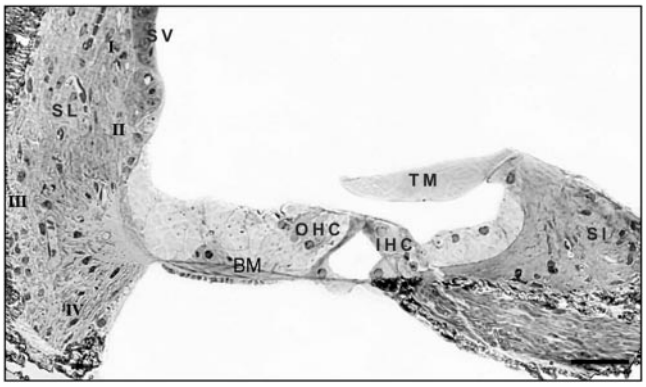

FIG. 5. Classification of cochlear fibrocytes. Shown is a semithin section in the sagittal orientation of the cochlea from an *Otos*$^{-/-}$ mouse stained with toluidine blue. In the spiral ligament (SL), type I (behind the stria vascularis [SV]), type II (below the spiral prominence), type III (lining the bony capsule), and type IV (in the triangular space inferior to the basilar crest) fibrocytes are shown. Fibrocytes are also present in the spiral limbus (Sl) and under the tectorial membrane (TM). The positions of an OHC and IHC are also indicated. Scale bar = 50 μm.

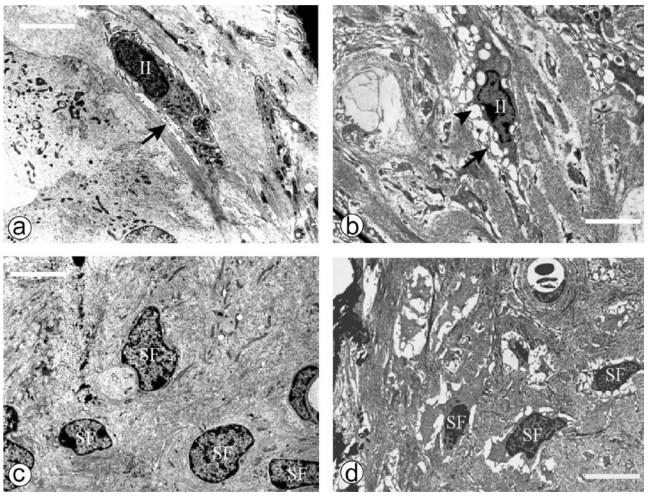

FIG. 6. Fibrocytes from spiral ligament and spiral limbus are damaged in *Otos*$^{-/-}$ mice. Shown are transmission electron micrographs of spiral ligament (a and b) and limbus (c and d) from wild-type (a and c) and *Otos*-deficient (b and d) mice. In the spiral ligament, both *Otos*$^{+/+}$ and *Otos*$^{-/-}$ type II fibrocytes (II mark) show normal membrane infoldings (arrows), but in *Otos*$^{-/-}$ mice (b), they exhibit numerous cytoplasmic vacuoles (arrowhead) and retraction of the cytoplasm and their nucleus appears as in first stage of apoptosis. In spiral limbus, fibrocytes (SF) from *Otos*$^{-/-}$ mice (d) show the same aspects of cytoplasm and nucleus, although with somewhat less vacuoles than in their spiral ligament counterparts, while fibrocytes of *Otos*$^{+/+}$ mice have a normal ultrastructure. Scale bars = 5 μm.

brane infoldings in fibrocytes suggests a diminished metabolism. These mice are severely deaf, as are human DFN3 patients with mutation in the *BRN4* gene. Although it is not known what function of the fibrocytes is impaired, it is likely that the production of some component of the endolymph is also abnormal, since there is a dramatic reduction in endocochlear potential. In *Otos*$^{-/-}$ fibrocytes, we observed changes that more or less resemble those of both *Slc12a2*$^{-/-}$ and *Pou3f4*$^{-/-}$ mouse models, but it is clear that the moderate auditory dysfunction found in *Otos*$^{-/-}$ mice implies a more subtle pathogenic mechanism than that in play in *Slc12a2*$^{-/-}$ and *Pou3f4*$^{-/-}$ mice.

Pathological processes with moderate functional impairment are age-related auditory loss (presbyacusis). Mouse models of presbyacusis have shown IHC and OHC loss with neuronal loss and alterations of the stria vascularis and fibrocytes. In these models, there are indications that damage to the lateral wall of the cochlea (i.e., stria vascularis and fibrocytes) could be an early event preceding the loss of hair cells and therefore be a primary cause of the pathology (9, 29). In the quiet-aged gerbil model (29), many vacuoles are observed in type II fibrocytes along with an increase in their surrounding extracellular spaces, presumably a sign of edema. These features of fibrocyte alteration along with moderate auditory impairment resemble the pathology occurring in *Otos*$^{-/-}$ mice. Thus, it is reasonable to address the question of whether the alteration of fibrocytes seen in *Otos*$^{-/-}$ mice leads to more profound changes in cochlear function and ultrastructure with time, such as hair cell and neuronal loss. This awaits backcrossing of *Otos*$^{-/-}$ mice on another genetic background to avoid the age-related hearing loss that occurs in C57BL/6N and 129 Olahsd-related strains.

In conclusion, we have shown that the lack of otospiralin leads to fibrocyte alterations and hearing impairment, enhancing the importance of the nonsensory regions of the cochlea in auditory function.

ACKNOWLEDGMENTS

We thank Harold Cremer (CNRS UMR 6156, IBDM, Marseille, France) for providing ES cells and Marie-Christine Simmler (INSERM U. 587, Paris, France) for giving us the *LacZneo* cassette. Blastocyste injection and chimeras were obtained at the Plateforme de Recombinaison Homologue in the Cochin Institute (INSERM). Animals were bred by Mireille Gallego. SEM and TEM were performed at CRIC (Centre Régional d'Imagerie Cellulaire) with the technical support of Chantal Cazevieille and Florence Tribillac. We thank Jean-Louis Pasquier for artwork.

This study was supported by grants from the Institut de la Santé et de la Recherche Médicale (INSERM). B.D. has a fellowship from Caisse d'Epargne, Montpellier, and Région Languedoc-Roussillon, France.

REFERENCES

1. **Cody, A. R., and I. J. Russell.** 1987. The response of hair cells in the basal turn of the guinea-pig cochlea to tones. J. Physiol. **383:**551–569.
2. **Cohen-Salmon, M., D. Frenz, W. Liu, E. Verpy, S. Voegeling, and C. Petit.** 2000. Fdp, a new fibrocyte-derived protein related to MIA/CD-RAP, has an in vitro effect on the early differentiation of the inner ear mesenchyme. J. Biol. Chem. **275:**40036–40041.
3. **Couloigner, V., M. Fay, S. Djelidi, N. Farman, B. Escoubet, I. Runembert, O. Sterkers, G. Friedlander, and E. Ferrary.** 2001. Location and function of the epithelial Na channel in the cochlea. Am. J. Physiol. Renal Physiol. **280:** F214–F222.
4. **Delprat, B., A. Boulanger, J. Wang, V. Beaudoin, M. J. Guitton, S. Venteo, C. J. Dechesne, R. Pujol, M. Lavigne-Rebillard, J.-L. Puel, and C. P. Hamel.** 2002. Downregulation of otospiralin, a novel inner ear protein, causes hair cell degeneration and deafness. J. Neurosci. **22:**1718–1725.
5. **Everett, L. A., B. Glaser, J. C. Beck, J. R. Idol, A. Buchs, M. Heyman, F. Adawi, E. Hazani, E. Nassir, A. D. Baxevanis, V. C. Sheffield, and E. D. Green.** 1997. Pendred syndrome is caused by mutations in a putative sulphate transporter gene (PDS). Nat. Genet. **17:**411–422.
6. **Everett, L. A., H. Morsli, D. K. Wu, and E. D. Green.** 1999. Expression pattern of the mouse ortholog of the Pendred's syndrome gene (Pds) suggests a key role for pendrin in the inner ear. Proc. Natl. Acad. Sci. USA **96:**9727–9732.
7. **Forge, A., D. Becker, S. Casalotti, J. Edwards, W. H. Evans, N. Lench, and M. Souter.** 1999. Gap junctions and connexin expression in the inner ear. Novartis Found. Symp. **219:**134–156.
8. **Henson, M. M., and O. W. Henson.** 1988. Tension fibroblasts and the connective tissue matrix of the spiral ligament. Hear. Res. **35:**237–258.
9. **Hequembourg, S., and M. C. Liberman.** 2001. Spiral ligament pathology: a major aspect of age-related cochlear degeneration in C57BL/6 mice. J. Assoc. Res. Otolaryngol. **2:**118–129.
10. **Kikuchi, T., R. S. Kimura, D. L. Paul, T. Takasaka, and J. C. Adams.** 2000. Gap junction systems in the mammalian cochlea. Brain Res. Brain Res. Rev. **32:**163–166.
11. **Laemmli, U. K.** 1970. Cleavage of structural proteins during the assembly of the head of bacteriophage T4. Nature **227:**680–685.
12. **Lautermann, J., W. J. Ten Cate, P. Altenhoff, R. Grummer, O. Traub, H. Frank, K. Jahnke, and E. Winterhager.** 1998. Expression of the gap-junction connexins 26 and 30 in the rat cochlea. Cell Tissue Res. **294:**415–420.
13. **Lavigne-Rebillard, M., B. Delprat, M.-O. Surget, J.-M. Griffoin, D. Weil, M. Arbones, R. Vincent, and C. P. Hamel.** 2003. Gene structure, chromosomal localization, and mutation screening of the human gene for the inner ear protein otospiralin. Neurogenetics **4:**137–140.
14. **Minowa, O., K. Ikeda, Y. Sugitani, T. Oshima, S. Nakai, Y. Katori, M. Suzuki, M. Furukawa, T. Kawase, Y. Zheng, M. Ogura, Y. Asada, K. Watanabe, H. Yamanaka, S. Gotoh, M. Nishi-Takeshima, T. Sugimoto, T. Kikuchi, T. Takasaka, and T. Noda.** 1999. Altered cochlear fibrocytes in a mouse model of DFN3 nonsyndromic deafness. Science **285:**1408–1411.
15. **Mothe, A. J., and I. R. Brown.** 2001. Expression of mRNA encoding extracellular matrix glycoproteins SPARC and SC1 is temporally and spatially regulated in the developing cochlea of the rat inner ear. Hear. Res. **155:** 161–174.
16. **Pace, A. J., V. J. Madden, O. W. Henson, B. H. Koller, and M. M. Henson.** 2001. Ultrastructure of the inner ear of NKCC1-deficient mice. Hear. Res. **156:**17–30.
17. **Patuzzi, R. B., G. K. Yates, and B. M. Johnstone.** 1989. The origin of the low-frequency microphonic in the first cochlear turn of guinea-pig. Hear. Res. **39:**177–188.

18. **Rendtorff, N. D., M. Frödin, T. Attié-Bitach, M. Vekemans, and N. Tommerup.** 2001. Identification and characterization of an inner ear-expressed human melanoma inhibitory activity (*MIA*)-like gene (*MIAL*) with a frequent polymorphism that abolishes translation. Genomics **71:**40–52.
19. **Robertson, N. G., L. Lu, S. Heller, S. N. Merchant, R. D. Eavey, M. McKenna, J. B. Nadol, R. T. Miyamoto, F. H. Linthicum, J. F. Lubianca Neto, A. J. Hudspeth, C. E. Seidman, C. C. Morton, and J. G. Seidman.** 1998. Mutations in a novel cochlear gene cause DFNA9, a human nonsyndromic deafness with vestibular dysfunction. Nat. Genet. **20:**299–303.
20. **Robertson, N. G., S. Heller, J. S. Lin, B. L. Resendes, S. Weremowicz, C. S. Denis, A. M. Bell, A. J. Hudspeth, and C. C. Morton.** 2000. A novel conserved cochlear gene, OTOR: identification, expression analysis, and chromosomal mapping. Genomics **66:**242–248.
21. **Sakaguchi, N., J. J. Crouch, C. Lytle, and B. A. Schulte.** 1998. Na-K-Cl cotransporter expression in the developing and senescent gerbil cochlea. Hear. Res. **118:**114–122.
22. **Schagger, H., and G. von Jagow.** 1987. Tricine-sodium dodecyl sulfate-polyacrylamide gel electrophoresis for the separation of proteins in the range from 1 to 100 kDa. Anal. Biochem. **166:**368–379.
23. **Scott, D. A., R. Wang, T. M. Kreman, V. C. Sheffield, and L. P. Karniski.** 1999. The Pendred syndrome gene encodes a chloride-iodide transport protein. Nat. Genet. **21:**440–443.
24. **Soto-Prior, A., M. Lavigne-Rebillard, M. Lenoir, C. Ripoll, G. Rebillard, P. Vago, R. Pujol, and C. P. Hamel.** 1997. Identification of preferentially expressed cochlear genes by systematic sequencing of a rat cochlea cDNA library. Mol. Brain Res. **47:**1–10.
25. **Spicer, S. S., B. A. Schulte, and J. C. Adams.** 1990. Immunolocalization of Na+,K(+)-ATPase and carbonic anhydrase in the gerbil's vestibular system. Hear. Res. **43:**205–217.
26. **Spicer, S. S., and B. A. Schulte.** 1991. Differentiation of inner ear fibrocytes according to their ion transport related activity. Hear. Res. **56:**53–64.
27. **Spicer, S. S., M. A. Gratton, and B. A. Schulte.** 1997. Expression patterns of ion transport enzymes in spiral ligament fibrocytes change in relation to strial atrophy in the aged gerbil cochlea. Hear. Res. **111:**93–102.
28. **Spicer, S. S., and B. A. Schulte.** 1998. Evidence for a medial K+ recycling pathway from inner hair cells. Hear. Res. **118:**1–12.
29. **Spicer, S. S., and B. A. Schulte.** 2002. Spiral ligament pathology in quiet-aged gerbils. Hear. Res. **172:**172–185.
30. **Stankovic, K. M., J. C. Adams, and D. Brown.** 1995. Immunolocalization of aquaporin CHIP in the guinea pig inner ear. Am. J. Physiol. **269:**C1450–C1456.
31. **Thomadakis, G., L. N. Ramoshebi, J. Crooks, D. C. Rueger, and U. Ripamonti.** 1999. Immunolocalization of Bone Morphogenetic Protein-2 and -3 and Osteogenic Protein-1 during murine tooth root morphogenesis and in other craniofacial structures. Eur. J. Oral Sci. **107:**368–377.
32. **Towbin, H., T. Staehelin, and J. Gordon.** 1979. Electrophoretic transfer of proteins from polyacrylamide gels to nitrocellulose sheets: procedure and some applications. Proc. Natl. Acad. Sci. USA **76:**4350–4354.
33. **Tsuprun, V., and P. Santi.** 1999. Ultrastructure and immunohistochemical identification of the extracellular matrix of the chinchilla cochlea. Hear. Res. **129:**35–49.
34. **Wangemann, P.** 2002. K+ cycling and the endocochlear potential. Hear. Res. **165:**1–9.
35. **Weinberger, D. G., W. J. Ten Cate, J. Lautermann, and M. Baethmann.** 1999. Localization of laminin isoforms in the guinea pig cochlea. Laryngoscope **109:**2001–2004.
36. **Wu, T., and D. C. Marcus.** 2003. Age-related changes in cochlear endolymphatic potassium and potential in CD-1 and CBA/CaJ mice. J. Assoc. Res. Otolaryngol. **4:**353–362.
37. **Xia, A. P., K. Ikeda, Y. Katori, T. Oshima, T. Kikuchi, and T. Takasaka.** 2000. Expression of connexin 31 in the developing mouse cochlea. Neuroreport **11:**2449–2453.
38. **Xia, A. P., T. Kikuchi, O. Minowa, Y. Katori, T. Oshima, T. Noda, and K. Ikeda.** 2002. Late-onset hearing loss in a mouse model of DFN3 non-syndromic deafness: morphologic and immunohistochemical analyses. Hear. Res. **166:**150–158.
39. **Zheng, Q. Y., K. R. Johnson, and L. C. Erway.** 1999. Assessment of hearing in 80 inbred strains of mice by ABR threshold analyses. Hear. Res. **130:**94–107.